

1N-70-CR

78202

p. 25

**FINAL REPORT  
MARSHALL SPACE FLIGHT CENTER  
CONTRACT # H-08082D& #H-11210D**

**"ADVANCED FLOW-POLISHING AND SURFACE  
METROLOGY OF THE S056 X-RAY TELESCOPE"**

**BAKER CONSULTING  
3/2/1992**

(NASA-CR-184318) ADVANCED FLOW-POLISHING  
AND SURFACE METROLOGY OF THE S056 X RAY  
TELESCOPE Final Report (Baker Consulting)  
25 p

CSCL 20C

N92-20515

G3/70    Unclass  
0078202

# Table of Contents

## Section 1.

### 1.1 Introduction.

1.1.1. Discussion of methods.

1.1.2. Presentation of previous data.

### 1.2 Interferometry and Surface Analysis.

1.2.1. Discussion of Metrology Set-up.

1.2.2. Data presentation pre-polish.

## Section 2.

### 2.1. Machine Set-up and parameters.

2.1.1. Standard Optical polishing.

2.1.2. Flow-Polishing.

### 2.2. In-Process Testing.

2.2.1. Interferometry methods.

2.2.2. Data Presentation.

## Section 3.

### Final Metrology.

3.1.1. Data Presentation

3.1.2. Comparison of Surface Contour.

## Section 4.

### Summary & Conclusions.

## 1.1. Introduction.

### 1.1.1 Discussion of methods

The surface finishing of X-ray grazing incidence optics is the most demanding area of optical processing, both in terms of metrology and application of optical finishing techniques.

During this contract the surfaces of an existing optical mirror was processed using a new removal technique that employs a jet of finely dispersed and extremely small particles that impact the surface producing, under the correct conditions, ultra-smooth surfaces, especially on aspheric curvatures. The surfaces of the SO56 mirror are tapered conical shapes that have a continuously changing radius with the primary mirror having a parabolic shape and the secondary a hyperbolic shape. Figure 1 shows the optical ray trace of this telescope.

SO56 Telescope System

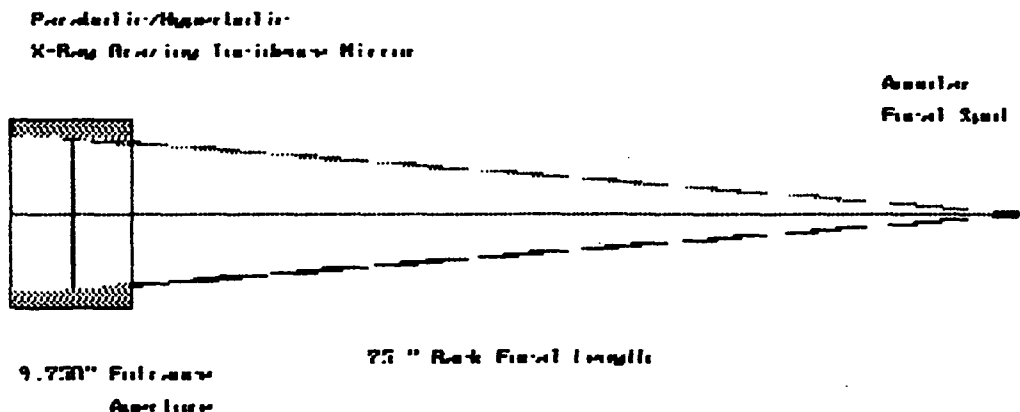


(Fig. (1) Theoretical Optical Ray-Trace of SO56 System)

The optical ray trace that was conducted on this telescope used the measured parameters from the existing substrates to set up the prescription for the optical layout. The optimization indicated a wavefront performance of  $.10 \lambda$  at  $.633 \mu$ . The following figure shows the isometric focal spot from this trace.

In figure 2 the focal spot has been produced from the random ray projection through the system falling onto the detector plane. The focal spot performance is indicative of an annular, obscured slit.

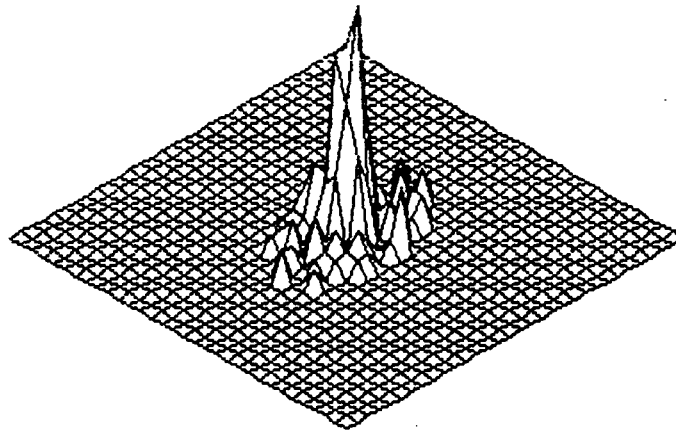


(Fig.(2). Blur Spot Theoretical Performance SO56.)

These first figures illustrate the nature of the surface that was flow-polished and attempt to convey the degree of difficulty that existed in maintaining the contour of the surfaces, while improving the smoothness. The use of Flow-Polishing is advantageous on these surfaces due to the grazing angle at which the jet can impinge on the surface.

The requirements of the contract were to measure the existing surface roughness and contour interferometrically and to improve, if possible, the roughness condition of the mirrors while maintaining, or improving the wavefront performance of the system.

#### 1.1.2. Presentation of Previous Data

The system was first measured using an unequal path Twyman Green (LUPI) interferometer, with the interferometer diverger conjugate confocal with the telescope overfilling the aperture of the telescope and then retro-reflecting from the precision test flat to be returned for interference with the reference mirror. Figure 3 illustrates this interferometric set-up.

The interferometer in figure 3 utilized a tilted spherical mirror in the output arm to produce a flattened fringe view in the horizontal plane. This allowed a more meaningful interpretation of the fringe extent.

Not shown in figure 3 is the use of multiple-pass interferometry that increases the sensitivity of the test. Due to the easily discernible error in the system it was not deemed necessary to use this test.

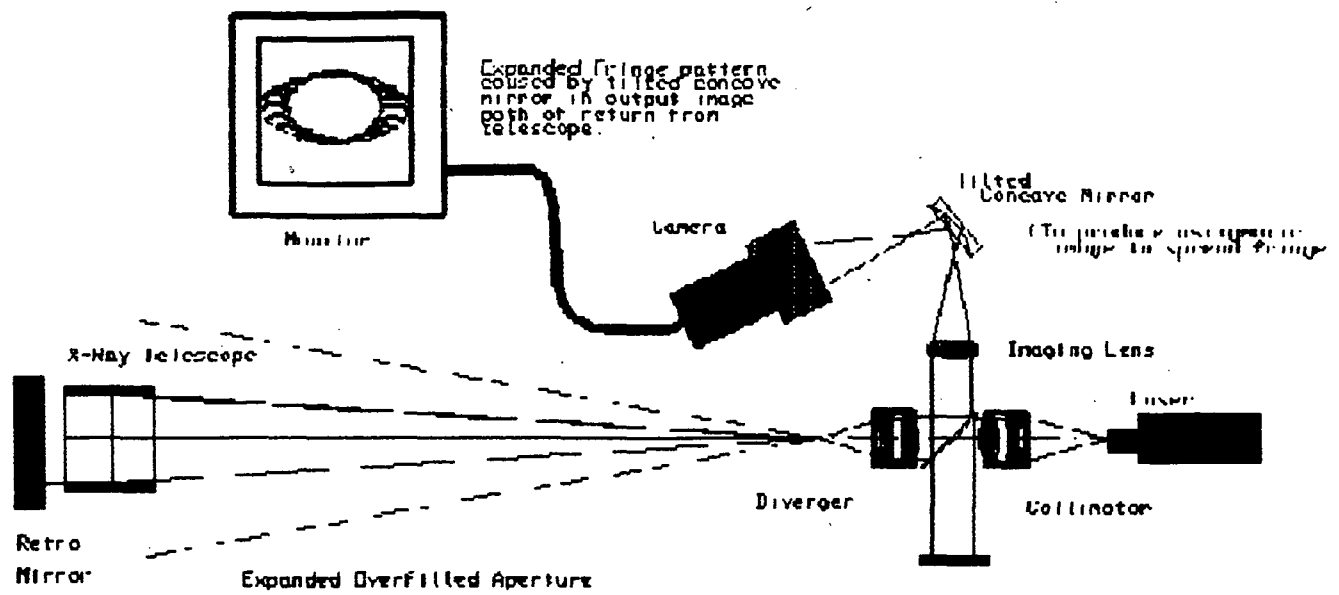


(Fig. (3). Twyman-Green Unequal Path Interferometer)

The initial interferometric tests showed over 2 waves of spherical aberration, with large astigmatic error as well. The astigmatism is due to two possible sources, out-of-roundness and mis-alignment. This data is shown in figure 4 and 5.

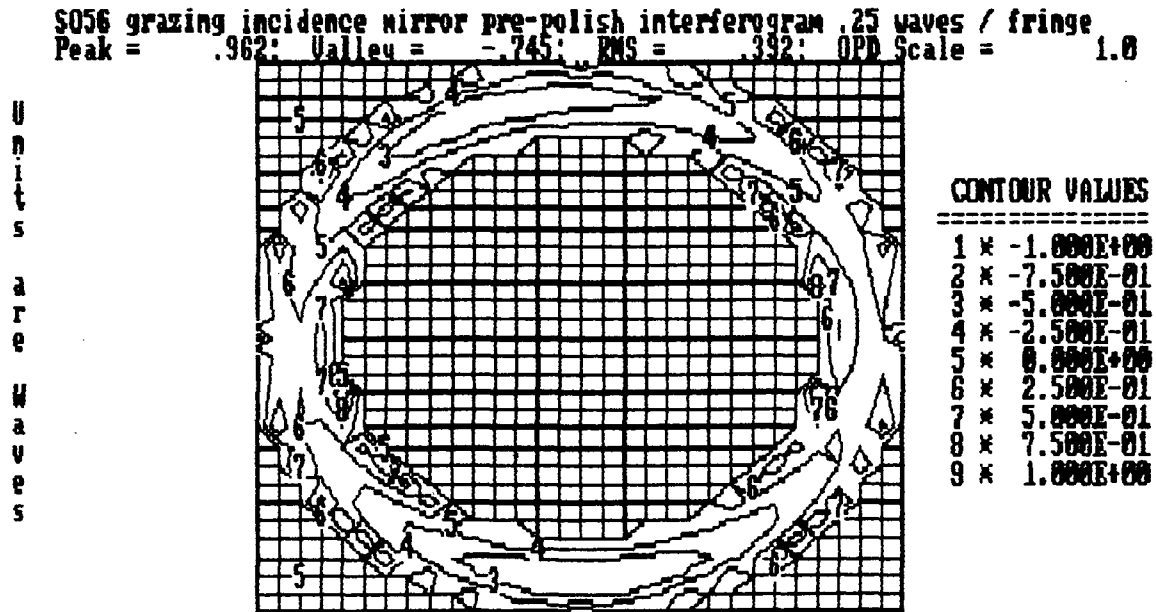
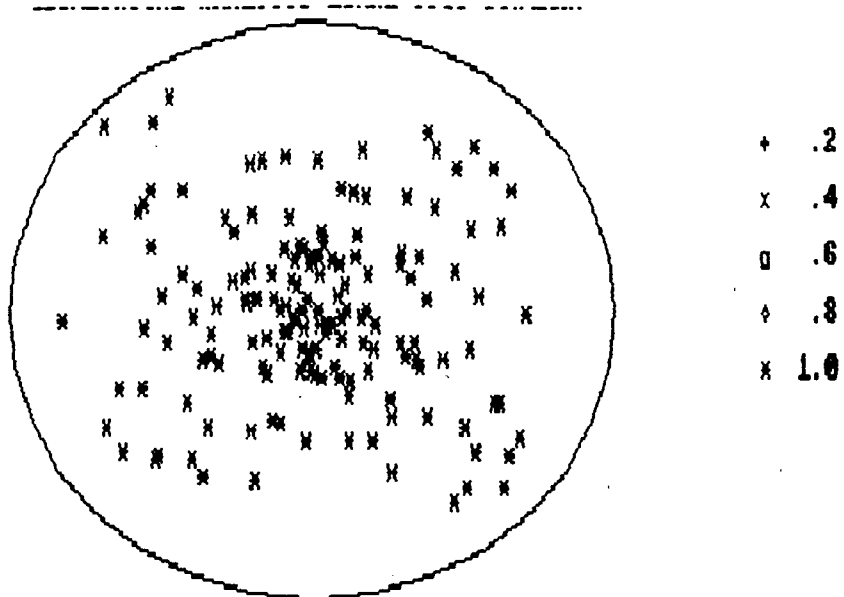


(Fig.(4.) Topographic plot of pre-Flow-Polish system.)



RAD=15.00: RMS RAD= 3.53 (Airy Radii) ANY KEY CONTINUE

(Fig. (5.) Blur Spot pre-Flow-Polish)

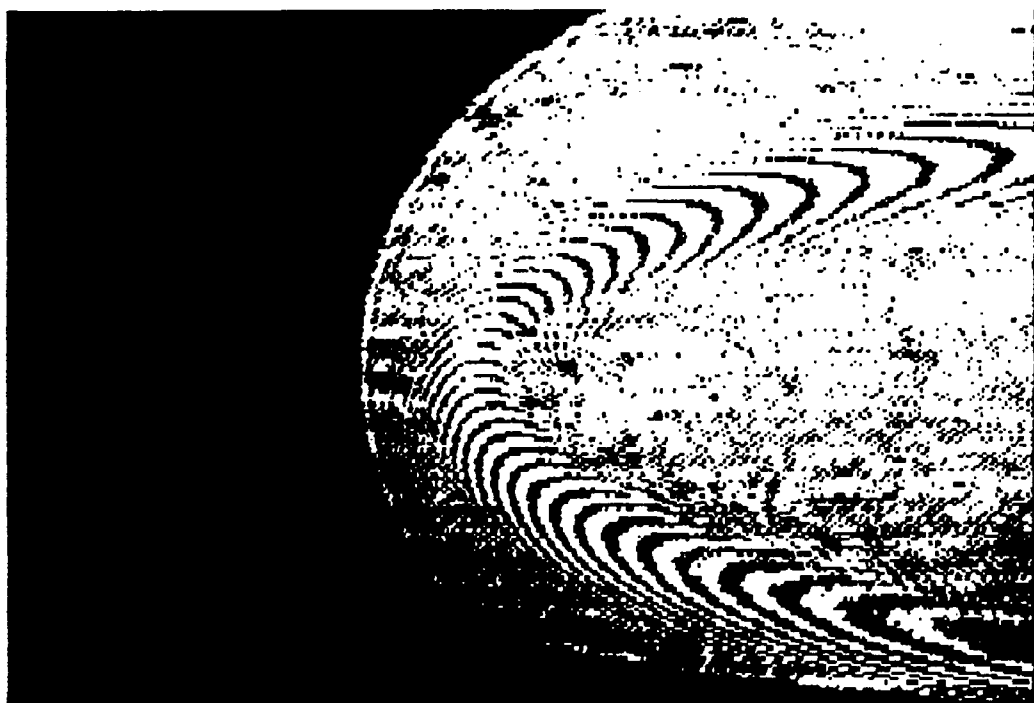


(Fig.(6).Extended Fringe View ,Fringes distortion a function of tilting interferometric image.)

The view in figure 6 was deliberately off-set to be able to clearly show the inner and outer edges of the fringe extent. This view does not show the full aperture. The interferogram in figure 5 shows this more clearly with the tilted concave mirror removed to show the non-distorted annular extent.

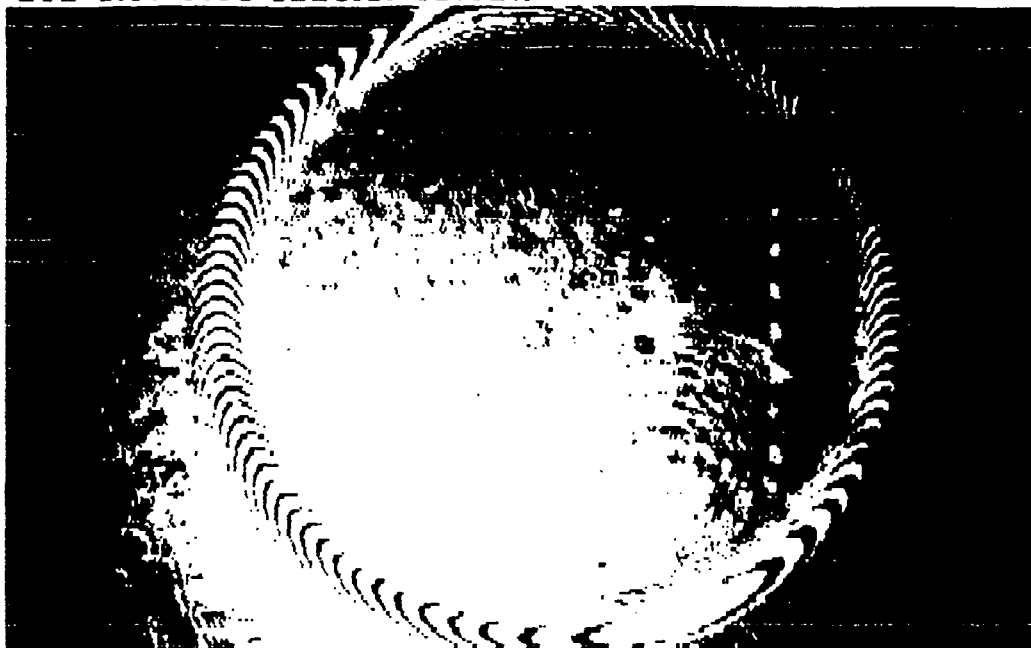


(Fig.(7). On-Axis Interferogram Showing Annular Aperture)

In figure (7) the full annulus is shown, the fringe detail is not nearly as pronounced as in figure 4. There is still strong spherical and the presence of astigmatism indicated in the non-symmetry of the full fringe pattern. the astigmatism is also irregular (skewed axis of astigmatism), making the use of any corrector negligible.

It is extremely difficult to correct for this out-of-roundness condition, the only available option is to attempt to correct the spherical as much as possible and not to exacerbate the existing roundness error.

The Flow-Polish treats a localized area and cannot average over large distances, the largest averaging area depends on the angle of impingement of the jet with respect to the work surface, as this area is extended too far the effective removal rate of the jet drops rapidly. This drop in removal versus averaging area is a critical factor in obtaining minimum surface roughness.

Due to this initial condition of high axial spherical and roundness error an initial contact technique was utilized to smooth and correct the wavefront error that existed in the surface. A combination of jet polish and close contact polish with a strong mechanical vibratory motion was applied in the first stages. Due to the confidential nature of this technique this will not be described in great detail in this report, only the data will be discussed.

An attempt to measure initial surface roughness was conducted on one of the two telescope elements. This measurement was done using BRDF techniques ,(Bi-Directional Distribution Function),.

The BRDF measurement is a light-scatter as a function of angle of impingement of visible collimated light .The wavelength was 633 nm (Helium-Neon). The results are shown in figure 8. It became clearly evident that the BRDF technique in its present optical arrangement would not produce meaningful data due to the nature of the strong cylindrical component that resulted from the reflection from the aspheric telescope surface.

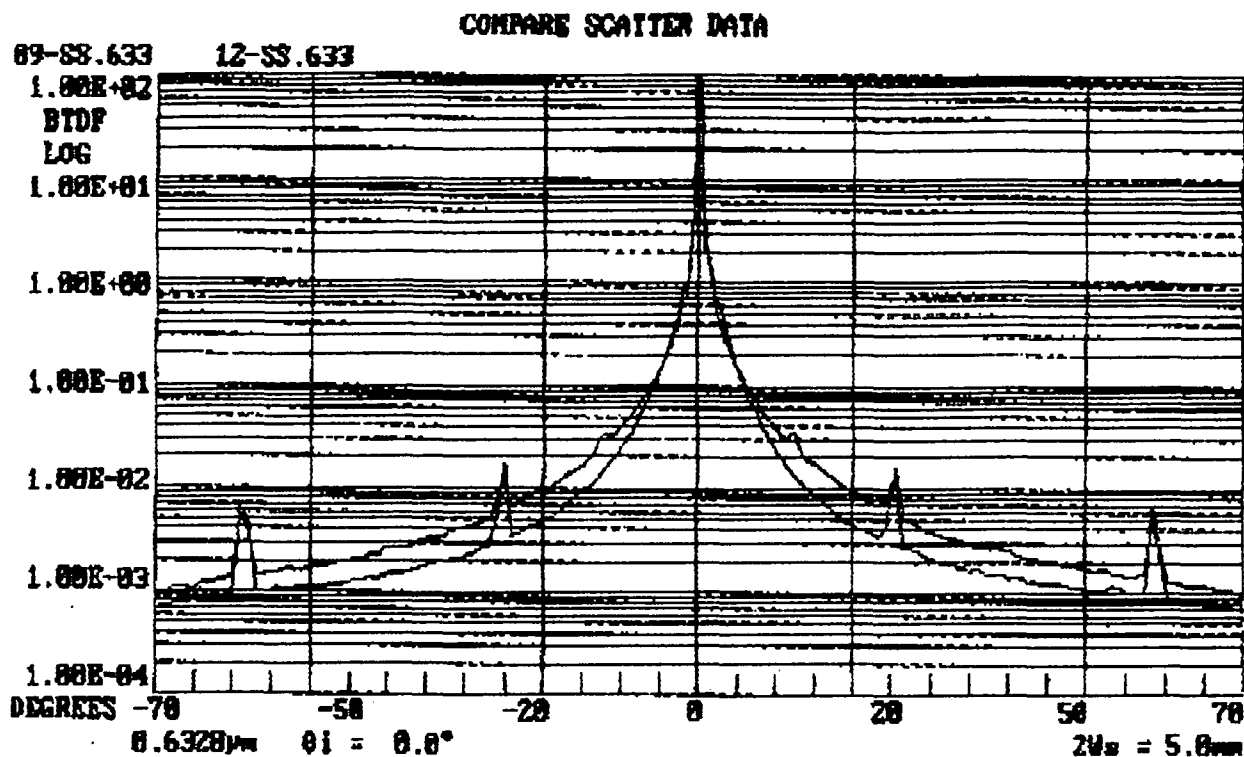


(Fig.(8).Pre-Flow Polish BRDF.)

The presence of strong spikes and and noise as well as two signal levels make interpretation of this data difficult. The average taken from the two signals has an average value of 1.00E-01. This would be roughly equivalent to a roughness value of 20-30 angstroms rms.

Several values were taken, however the signals were noisier than the data shown and would be redundant for this report.

Roughness data after the Near-Contact and Flow-Polish were also taken and will be shown in the final section of this report. The value of this type of measurement could be enhanced with changes in the systems optical configuration to accommodate grazing incidence surfaces.

## Section 2.

### 2.1 Machine Set-Up and Processing Parameters

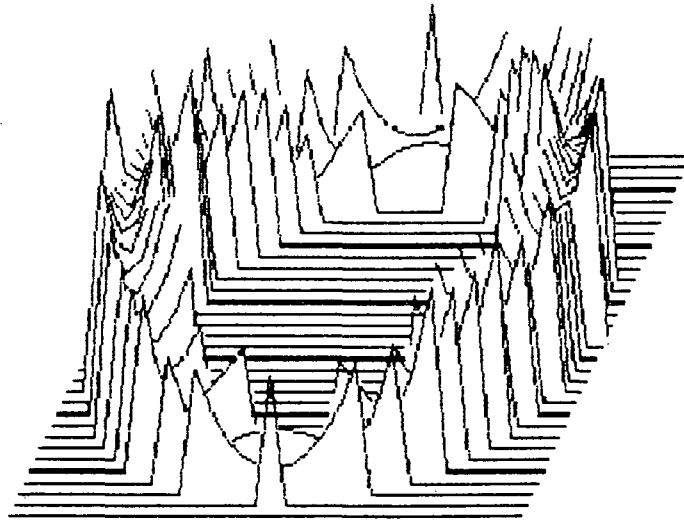
#### 2.1.1. Near-Contact -Polishing

As mentioned in the previous section a near-contact polishing method was applied to began the correction of the contour. While a full discussion of this technique can not be conducted in this report the results of this procedure and the initial data will be discussed.

In figures 4&9 the initial wavefront reduction is shown. This analysis was a result of digitizing the fringes from the orthoganol fringe pattern from figure 7.

S056 grazing incidence mirror pre-polish interferogram .25 waves / fringe  
Peak - .962; Valley - -.745; RMS - .392; OPD Scale - 1.8

U  
n  
i  
t  
s  
  
a  
r  
e  
  
W  
a  
v  
e  
s



View Angle = .8°

(Fig.(9). Isometric View of Pre-Flow-Polished System.)

The contour of the surfaces clearly shows spherical aberration with contributions from both surfaces and possibly from the relationship of one surface to the other with respect to final focus position.

The initial ray trace data indicated that a very small change in the conic constant perturbs the amount of spherical aberration and also shifts the focal position rather dramatically.

After this analysis the mirror system was worked iteratively by testing one against the other to determine any changes in the contour.

The near-contact method was continued until changes were made these changes were determined by the in-process testing using the extended fringe shape change as the figuring guide.

A more detailed discussion of the in-process testing will be covered in Section 2.2.

The figuring using the near-contact method was discontinued when it became evident that the overriding error in the system was the astigmatism. At this point the processing was switched to Flow-Polishing in the attempt to improve the surface roughness this is shown in figure 10.

### Flow-Polish of Grazing Incidence Mirror

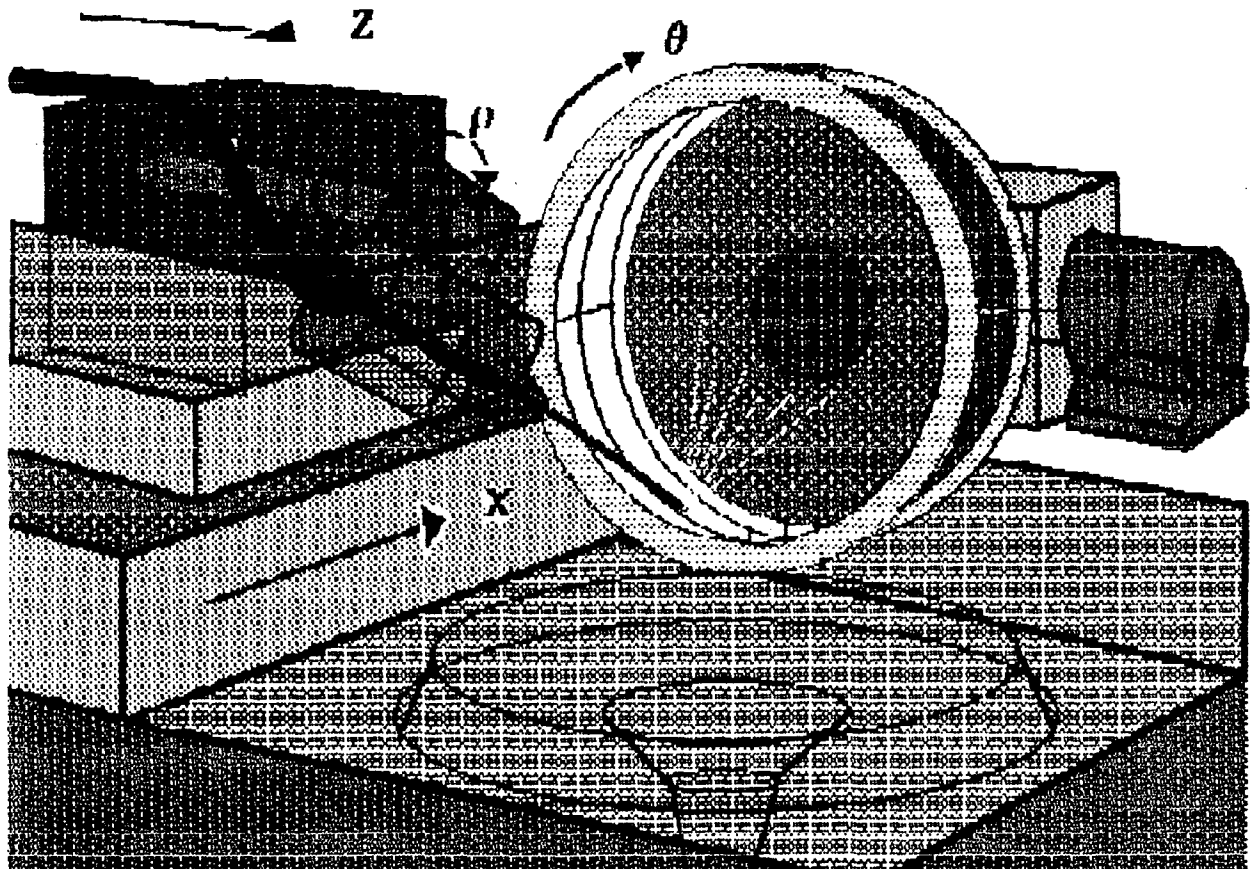


Fig. (10).  
(View of machine set-up for Flow-Polishing)

The Flow-Polish is done on a adjustable table to align the mirror for optimal tilt angle with respect to the machine. The impingement angle of the jet is adjusted by rotating the jet head through  $\rho$  until the conditions for removal are met. This is an iterative process for each new material.

The jet is then traversed across the surface in as smooth a manner as possible to maintain uniform removal of material. the part rotates at a very slow speed to allow the directional activity of the jet to act on the surface for maximum effect.

Both axis of movement are used X and Z are operated at varying speeds to cause a random location of the jet profile with respect to any transitory position on the surface.

Section 2.2 In-Process Testing

2.2.1 Interferometry Methods

In addition to the use of an un-equal path interferometer several other interferometric tests were used as in process tests. The most useful of these was a parallel plate shear test that sampled only a small part of the image. This test is shown in figure 11.

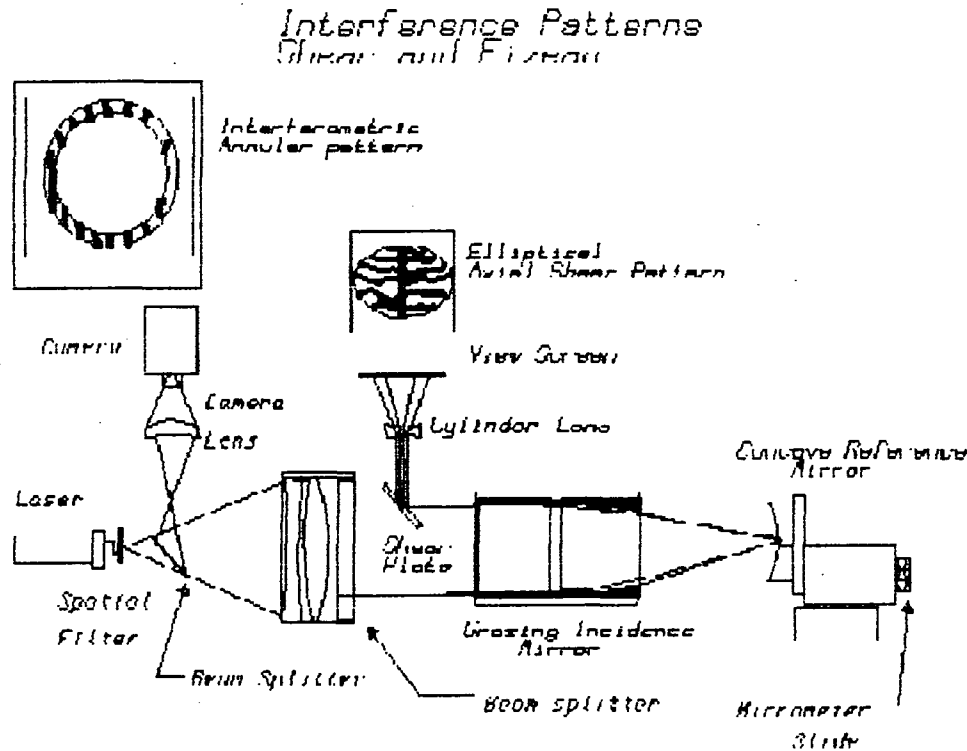


(Fig.(11).In-Process Interferometer Set-Up.)

In figure 11 a combination of interferometry is shown. The use of a collimated input beam allows several different arrangements for viewing or sampling interference or slope fringes.

This is valuable during in-process testing as it offers several cross checks for alignment and fringe interpretation during figuring of the optical surfaces.

### 2.2.2 Data Presentation

The interferogram in figure 12 shows a sampled pie-shaped segment using shearing slope interferometry. This is shown in figure 9 by the use of a collimated beam that is sheared by a parallel plate to create a lateral shear and also to spread the fringe extent over a large area. This changes the fringe aspect without affecting the wavefront value of the fringes.



(Fig.(12). Sampled Area Using Lateral Shear.)

This shearing technique allowed a rapid assessment of the local area along the axis of the wavefront changes. This lateral shear does not test both vertical and horizontal simultaneously, however it does test the axial contour efficiently and is relatively vibration free.

The other technique that was used during in-process was a local interferometric view using the Twyman-Green system. The results of this are shown in figure 13. The input cone angle of the interferometer was deliberately obscured in order to magnify a local area to more closely observe the interface between the hyperbola and the parabola.

This is shown in figure 13 where a section of the annulus is shown highly magnified to accentuate the normal extent across the slit.

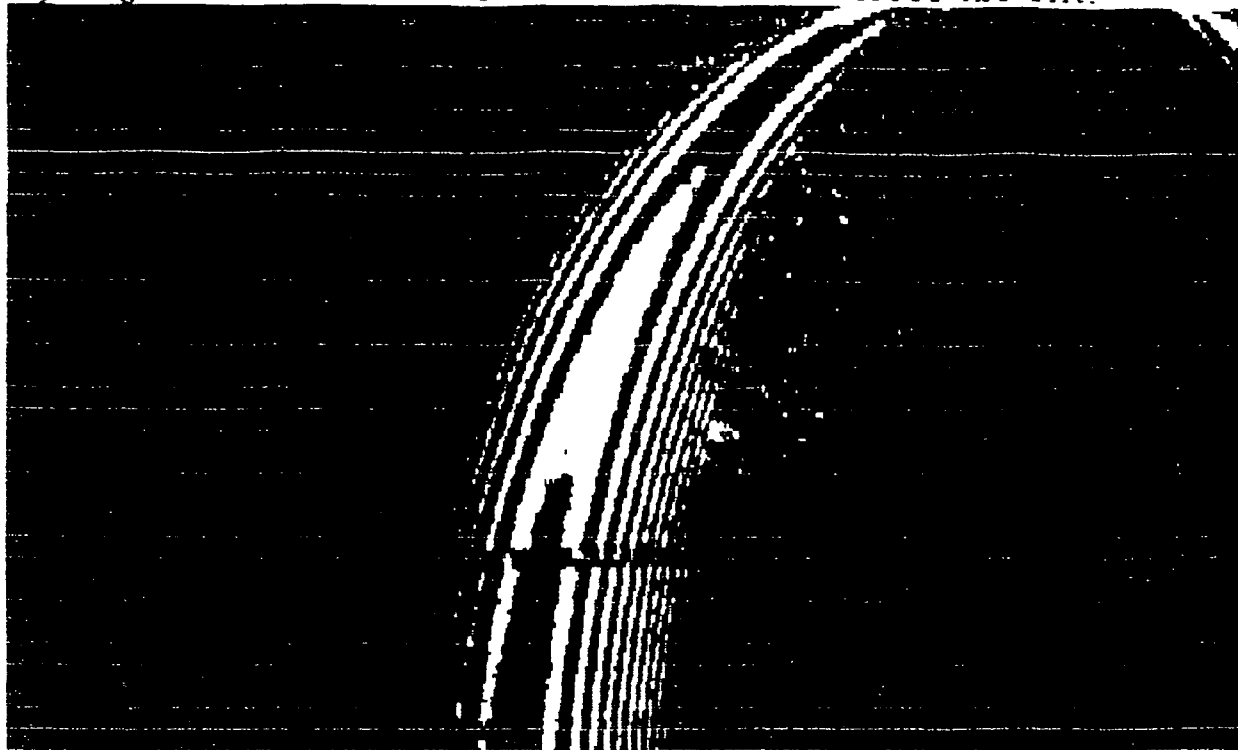


Fig.(13). Magnified Annular Interferogram.

In figure 13 the obscuration from the aperture spider can be clearly seen indicating sharp focusing through the system. This is important with regards to reducing diffraction effects in the image plane of the interferometer.

The in-process tests were not digitized for wavefront performance the fringe shape was a clear enough indicator during processing to show the progress. The final test was done using the Tyman-Green Interferometer with a normalized annular image.

The next section will cover the final data and the comparison of the pre-flow-polished versus the post flow polished analysis.

### Section 3

#### 3.1. Final Metrology

##### 3.1.1 Data Presentation

This section will cover the final analysis of the telescope system In figure(s) 12-20 the interferograms from the Tyman-Green on-axis tests have been digitized to produce the post Flow-Polished wavefront data.

Slope interferogram of so56 after flow polish  
 Peak = .443; Valley = -.326; RMS = .198; OPD Scale = 1.0

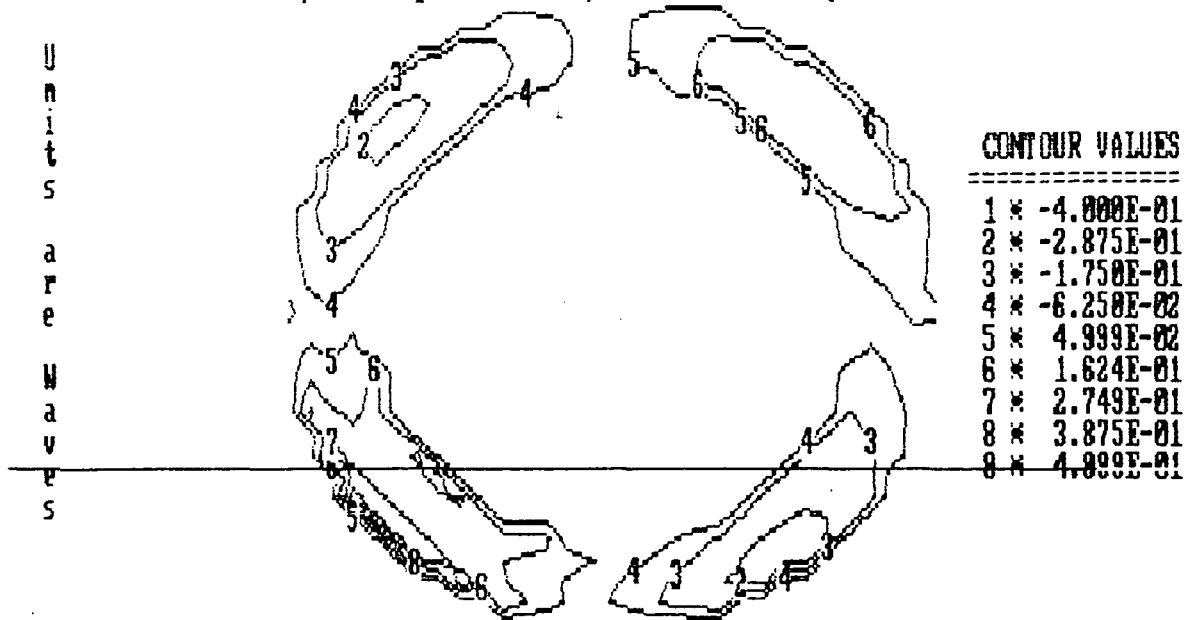
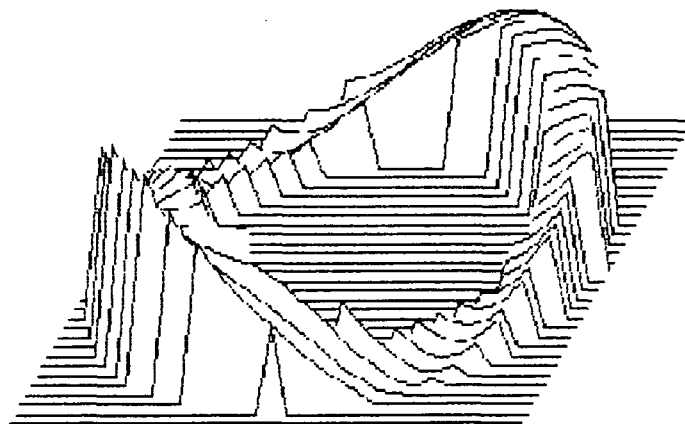


Fig.(14).  
 (Topographic Contour Plot of SO56 telescope mirror after final polishing values are in waves at 633 nm.)

Slope interferogram of so56 after flow polish  
 Peak = .443; Valley = -.326; RMS = .198; OPD Scale = 1.0

Units are Waves



(Fig.(15). Isometric View of Wavefront after Flow-Polish)

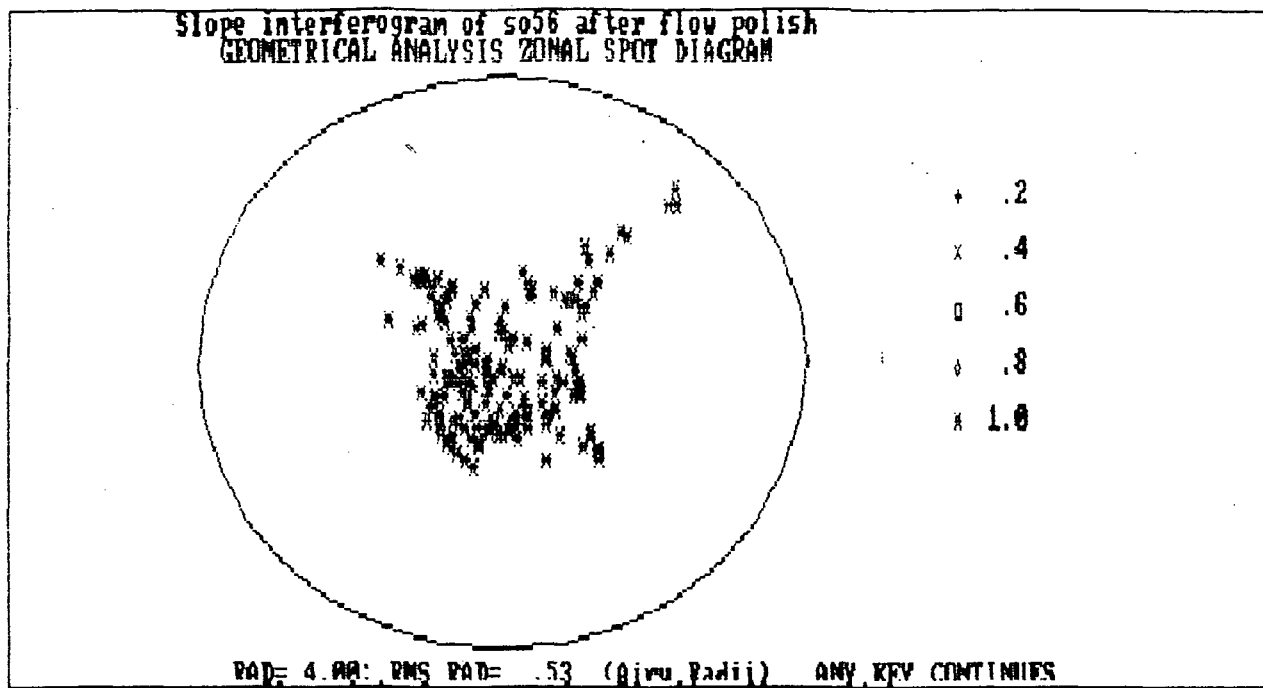


(Fig.(15) Blur Spot Analysis After Flow-Polish)

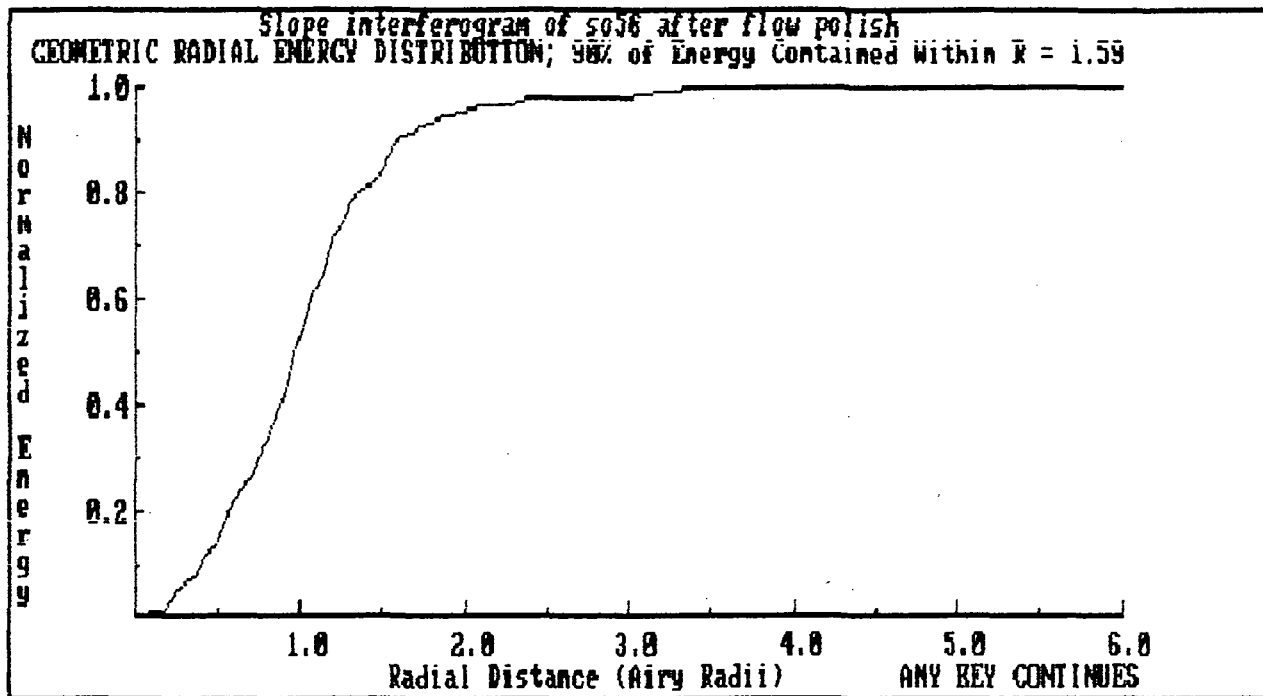


(Fig.(16). Radial Energy after Flow-Polish.)

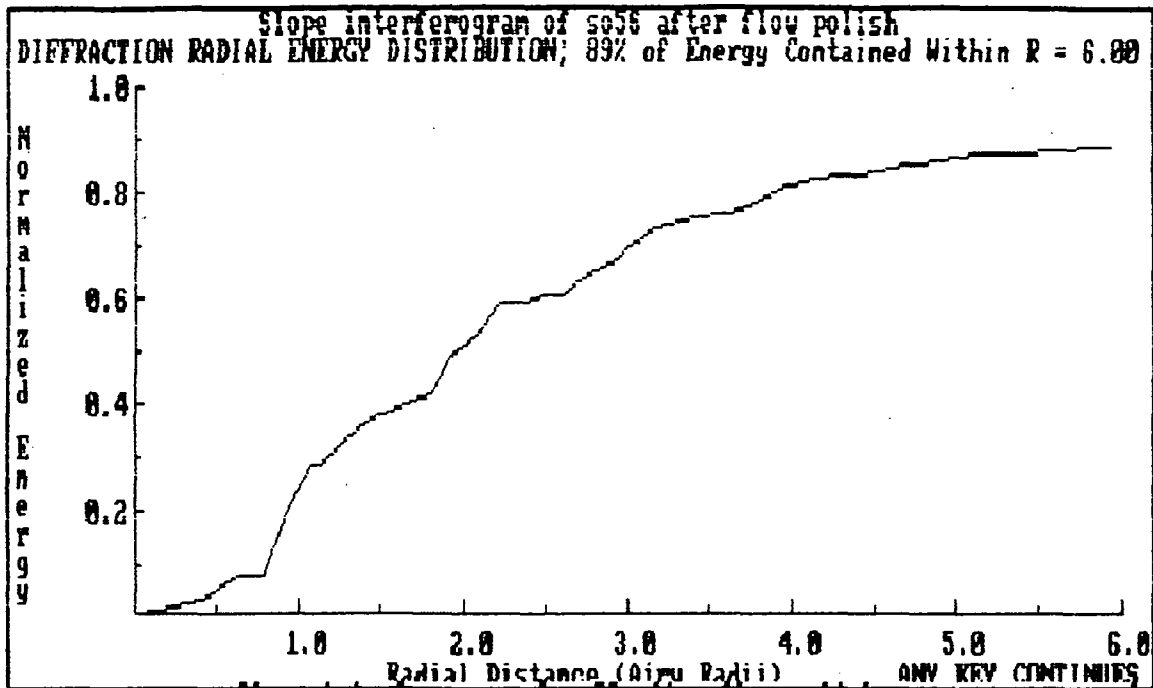


(Fig. (17) (Diffraction Radial Energy Measurement After Flow-Polish)

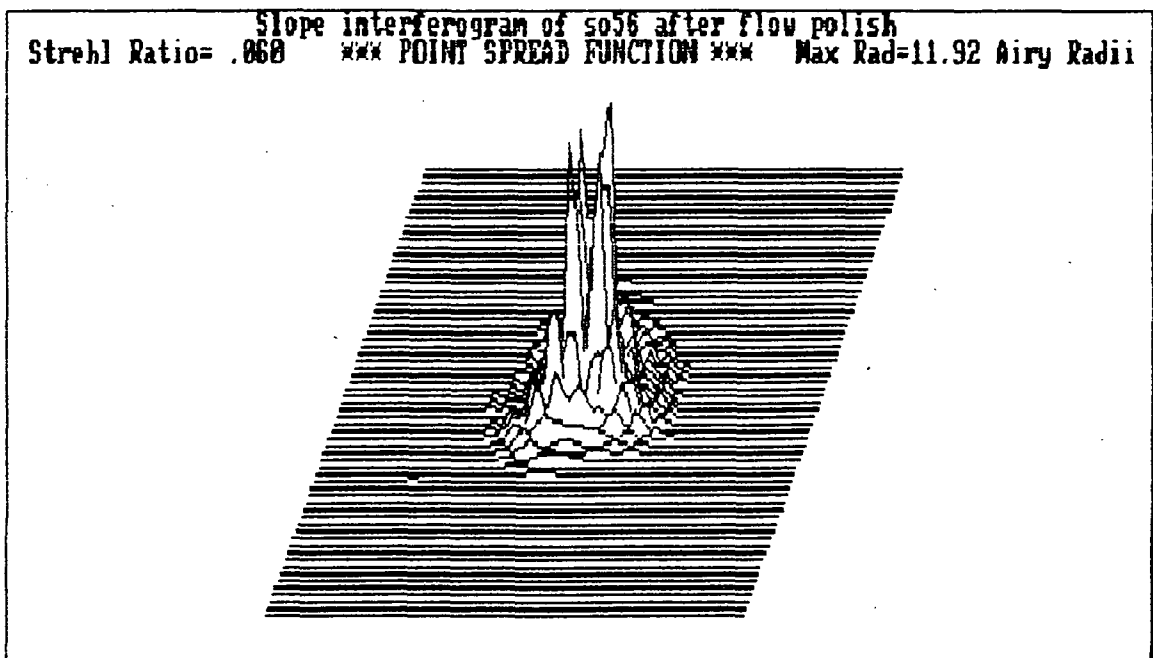


(Fig.(18). Point Spread Function of SO56 telescope after Flow-Polish (Note similarity to 2D profile in figure 2. on page 3. The wavefront error is similar)

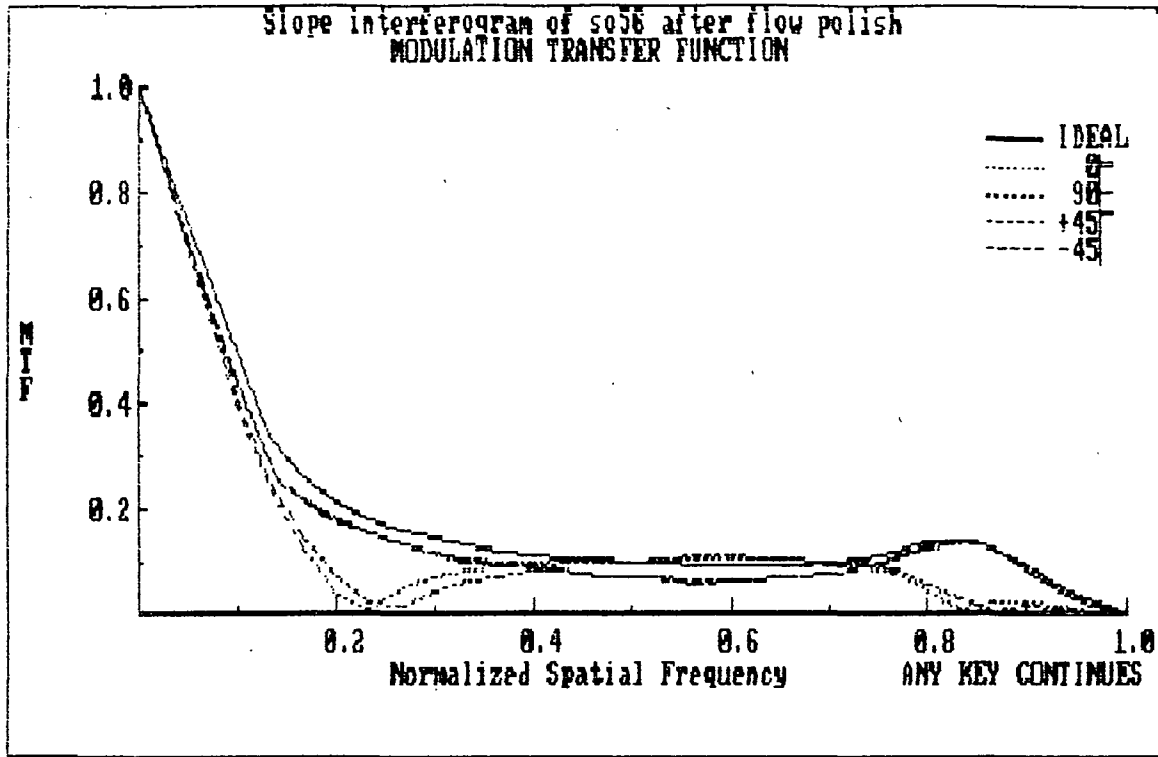


(Fig.(19) Modulation Transfer Function of SO56 After Flow-Polishing.)

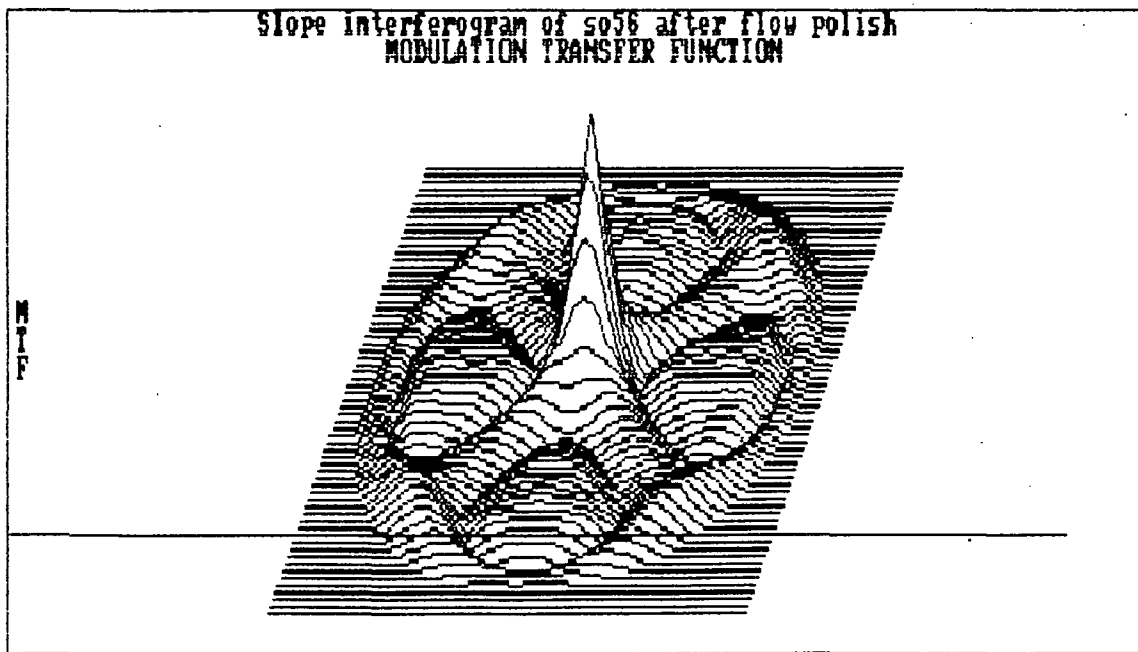


(Fig.(20). 3-D MTF Showing symmetry response due to the rotational error in the system.)

The previous post-Flow-Polished wavefront plots originated from the Twyman-Green Interferometer that produced the following interferograms. Both vertical and horizontal interferograms were digitized and the two optical path difference files were algebraically averaged in order to obtain the most meaningful information from the annular fringe extent.

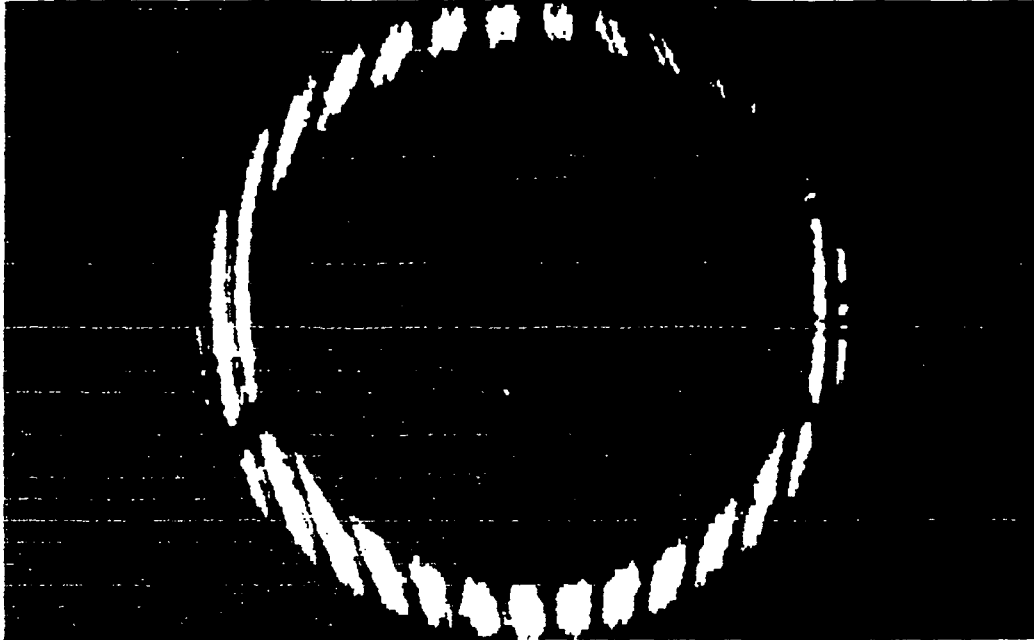


(Fig.(21). Interference fringes after Flow-Polishing vertical direction full annular aperture.)



(Fig.(22). Horizontal fringes from Twyman-Green Interferometer measurement.)

COMPARE SCATTER DATA

POLY84-5.63 POLY85-5.63

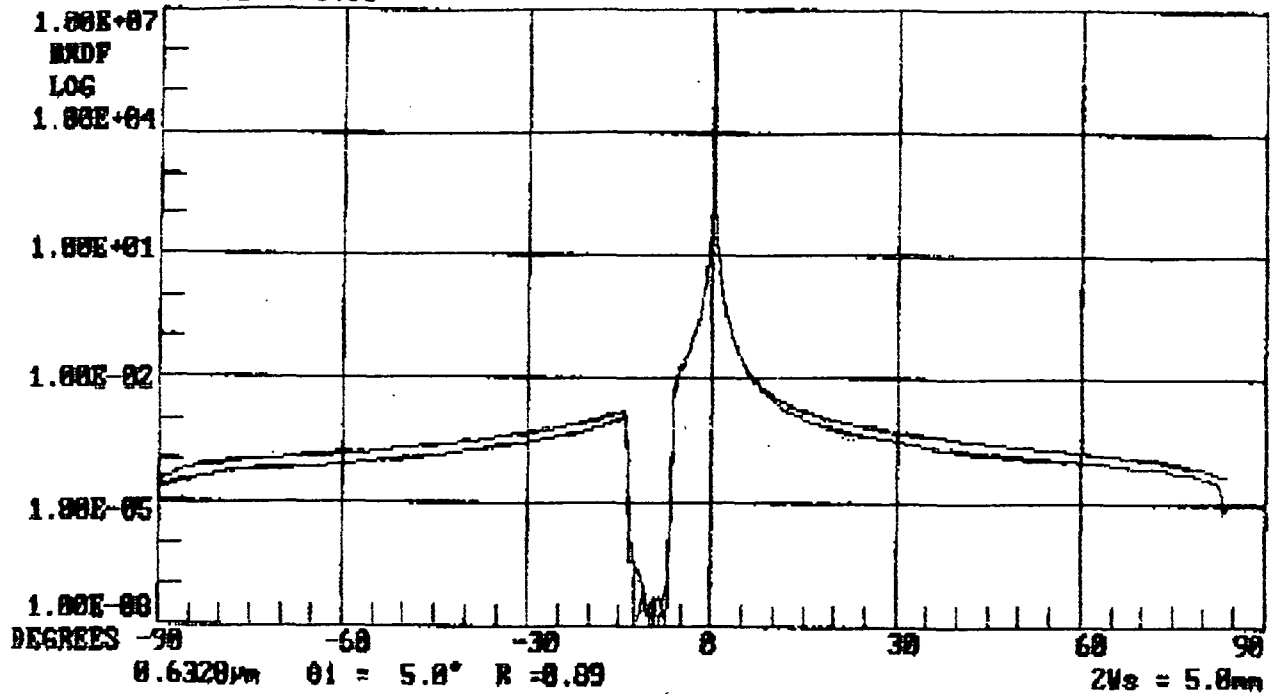


(Fig.(24). Post-Flow-Polish BRDF.)

In figure 23 the post-polish BRDF is shown for the SO56 surface of the paraboloid. The values are again noisy with a dip in the scatter value between -30 and +30 degrees. This is probably due to the signal not being available at the near normal angles. The values appear to indicate an improvement, however due to the nature of the signal it is questionable. The average value seems to be between  $1.00E-05$  and  $1.00E-03$ . This would indicate a surface that has a roughness of 5-10 angstroms rms.

While this looks like an improvement from a comparative sense the values are subject to the optical beam distortion caused by the strongly astigmatic profile from the grazing incidence surface.

A different optical configuration would have to be devised in order to achieve greater reliability and/or absolute comparisons.

There is also indications from studies done in the E.U.V. for BRDF techniques that the correlation between the visible and the E.U.V. and X-Ray regions is not well established. This was not known at the time of the work completed under this contract.

An alternate approach for future work would be to utilize an existing facility that can measure the hard-X-Ray scattering on systems such as the SO56 telescope. This facility is located at U.C. Berkeley. This measurement was outside the original scope of this project and was not attempted at this time.

### 3.1.2 Comparison of Surface Contours.

This final section will discuss and present data on the comparison of the pre and post Flow-Polish conditions. An interferometric difference has been constructed that shows the delta change between the pre and post condition. In figure 24 the topographic map is the delta contour change between pre and post operations.

The contour map shows the subtraction of the pre flow-polish contour from the post flow-polish contour. The changes that are seen be correlated to the reduction in wavefront error from pre to post.

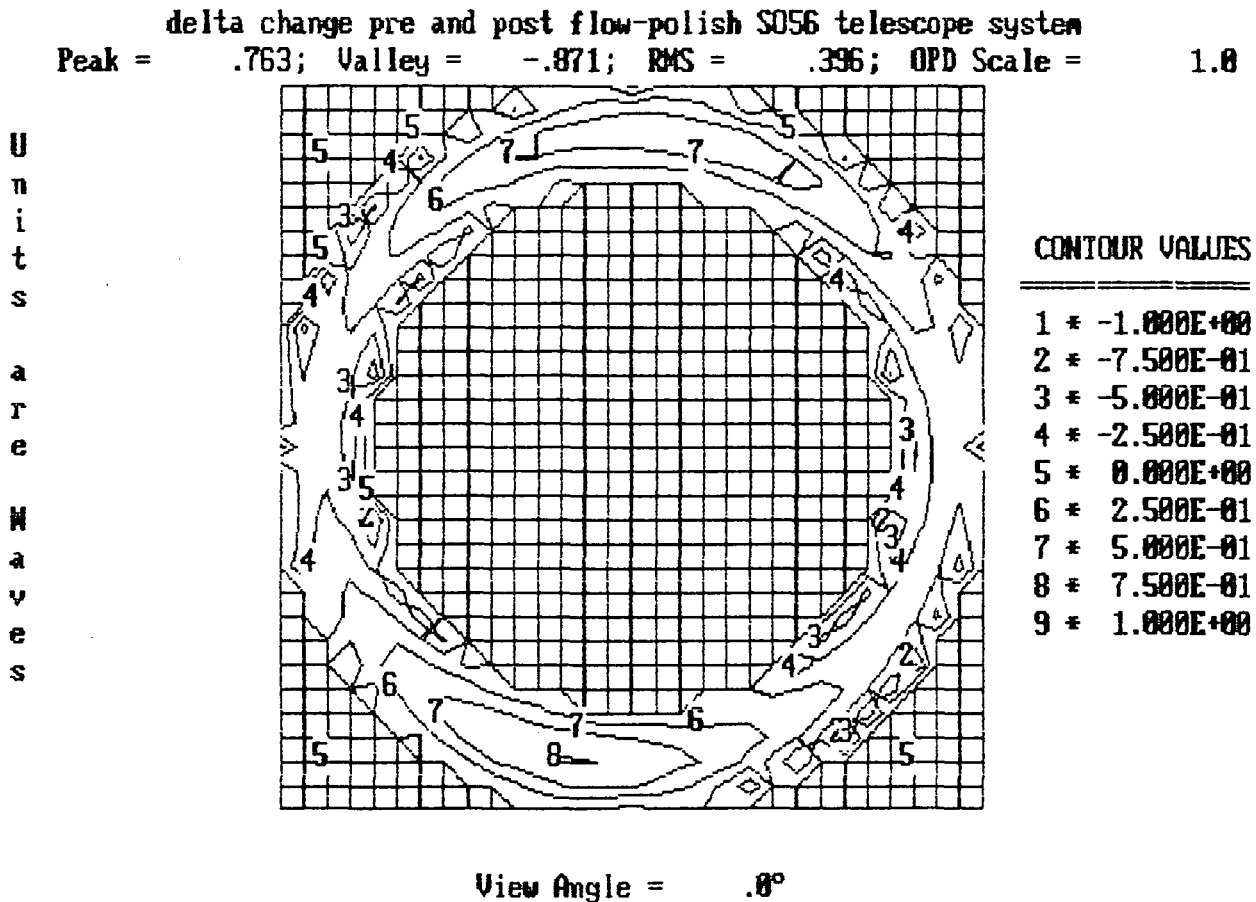
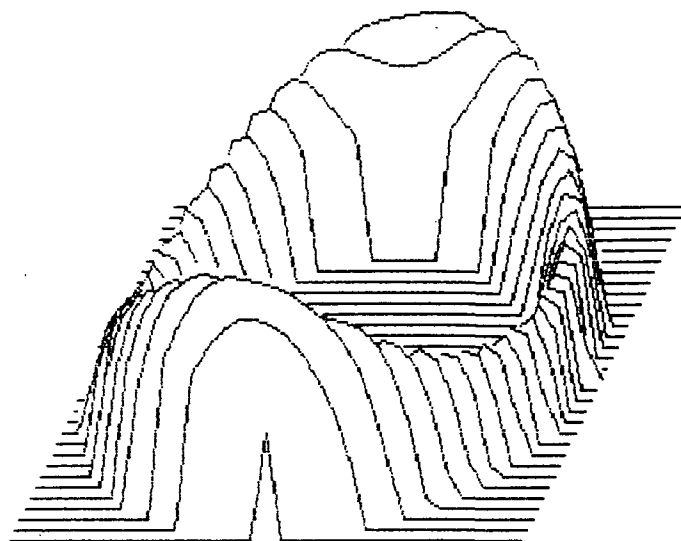


(Fig.(25). Topographic difference mapping of wavefront error.)

In figure 25 the isometric mapping of the contour difference is shown. The peak-to-valley error is shown in the topographic plot and in the isometric plot. the contour peak-to-valley change is  $1.6 \lambda$  at  $.6328 \mu$ . This value is the maximum change between the pre and post flow-polish wavefront maps.

delta change pre and post flow-polish S056 telescope system  
Peak = .763; Valley = -.871; RMS = .396; OPD Scale = 1.0

U  
n  
i  
t  
s  
  
a  
r  
e  
  
W  
a  
v  
e  
s



View Angle = .8°

---

(Fig.(26). Isometric View of Wavefront Difference Plot.)

The view in figure 26 indicates the reversal in the spherical aberration from the pre to post condition. For comparison look at figure 9 on page 7 and compare the slope changes between the plots.

The appearance of the roundness error has not changed, this was expected with the only difference being the axis of astigmatism appears to have swapped the positive and negative power directions. This is a possible function of the manner in which the Zernike Polynomial coefficients have been fitted due to the reversal in the spherical aberration.

Comparing the wavefront plot in figure 15 to both figure 9 and figure 25 the asymmetry manifests the same roundness condition.

In the interest of completeness the remaining figures show the wavefront difference effects on the Energy distribution, Modulation transfer function, Point spread function, and the Blur spot shape.

delta change pre and post flow-polish S056 telescope system  
 GEOMETRIC RADIAL ENERGY DISTRIBUTION; 59% of Energy Contained Within  $R = 6.00$

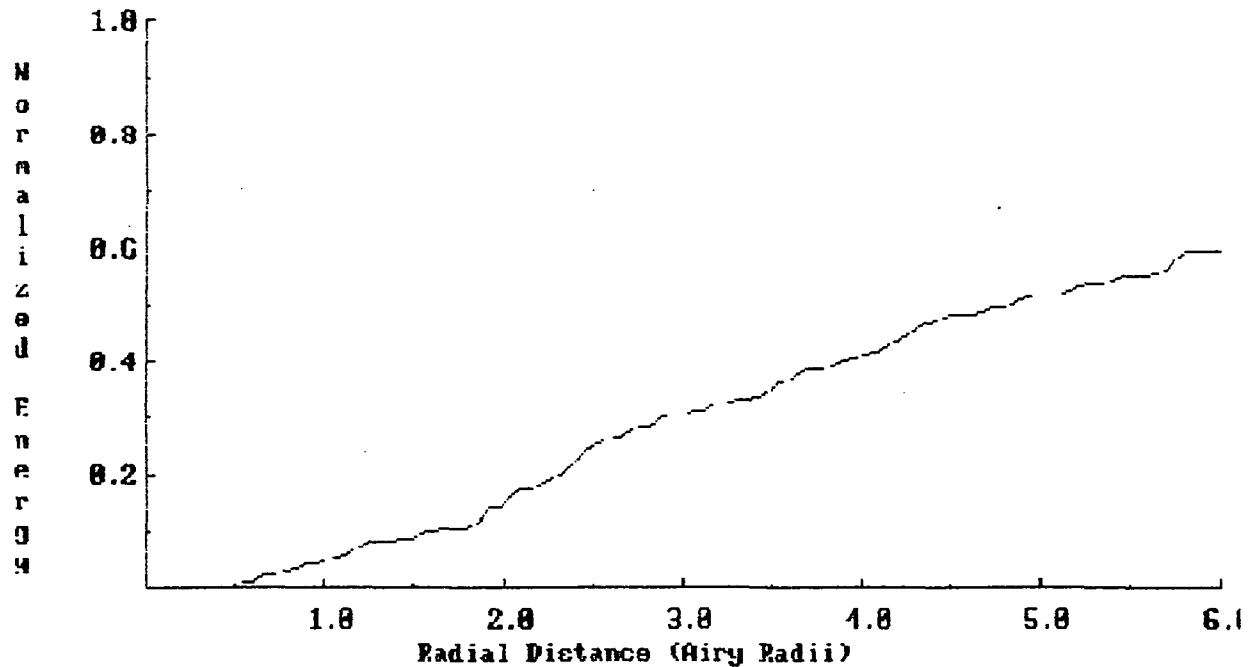


(Fig.(27). Geometric Radial Energy Distribution  
 Wavefront Difference Mapping)  
 delta change pre and post flow-polish S056 telescope system  
 MODULATION TRANSFER FUNCTION

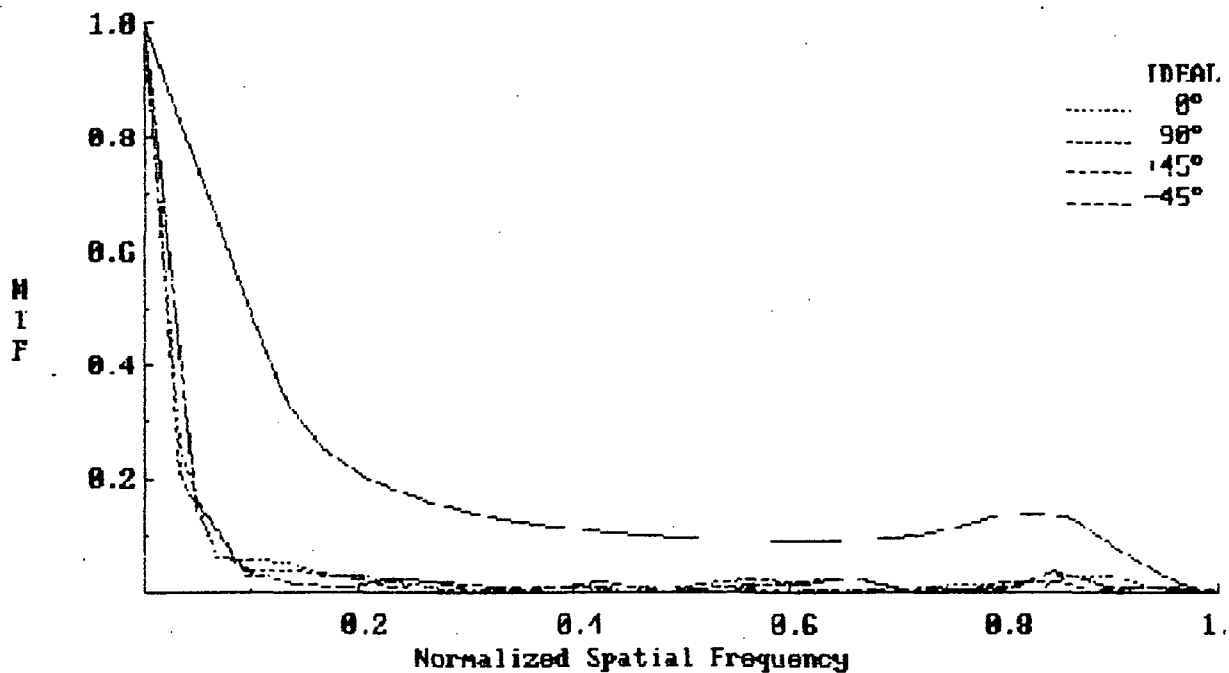


(Fig.(28). Modulation transfer Function Wavefront Difference)

delta change pre and post flow-polish S056 telescope system  
 Strehl Ratio= .008 \*\*\* POINT SPREAD FUNCTION \*\*\* Max Rad=11.92 Airy Radii

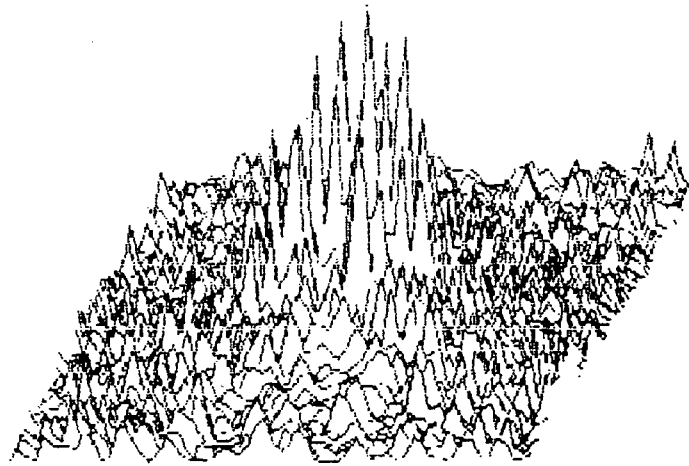


(Fig.(29). 3-D Point-Spread function of wavefront difference.)

delta change pre and post flow-polish S056 telescope system  
 DIFFRACTION RADIAL ENERGY DISTRIBUTION; 40% of Energy Contained Within  $K = 6.00$

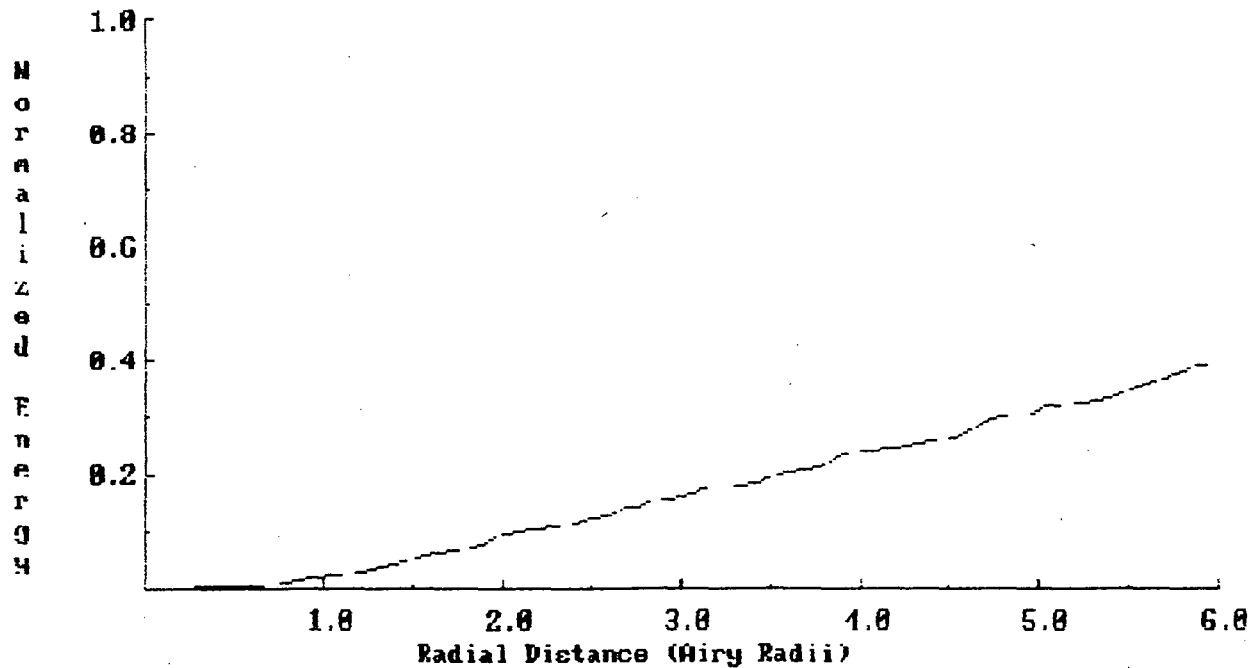
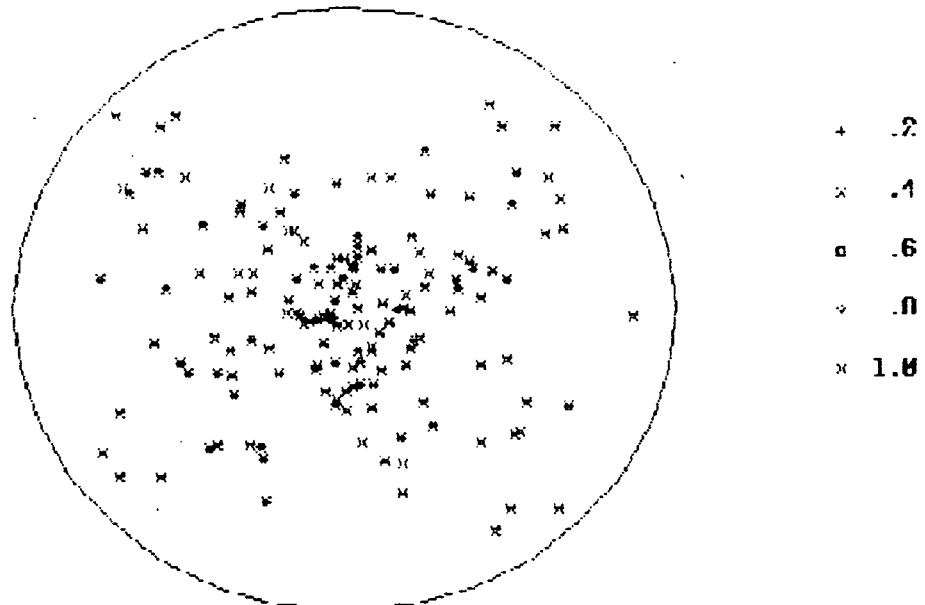


(Fig.(30). Diffraction Radial Energy Wavefront Difference.)

delta change pre and post flow-polish S056 telescope system  
 GEOMETRICAL ANALYSIS ZONAL SPOT DIAGRAM

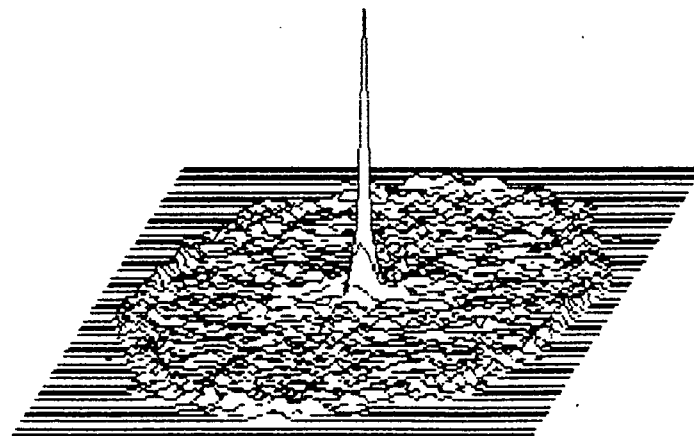


RAD-14.00; RMS RAD- 3.30 (Airy Radii)

(Fig.(31). Wavefront Blur Subtraction Pre and Post Flow-Polish.)

delta change pre and post flow-polish S056 telescope system  
 MODULATION TRANSFER FUNCTION

M  
I  
F



Normalized Spatial Frequency

(Fig.(32). 3-D MTF of Wavefront difference plots showing the residual MTF from pre and post subtraction.)

## Summary & Conclusions

The last 6 figures can be interpreted as the amount of fitted aberration error that has been removed per the analysis of the fringes from the pre and post interferograms. The interpretation has several sources of error, alignment differences between the pre and post testing, fringe detection errors on fringe centers, aperture pupil definition for the circular Zernike Polynomial fitting, and the wavefront data point fitting to the Zernike Polynomial expression.

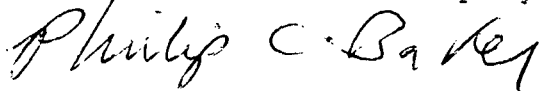
All of these error sources can skew the final data, however the appearance of the symmetry from analysis to analysis indicates that these errors are not significant in terms of the actual reduction of wavefront error from pre to post condition.

The possible improvement in surface roughness from the BRDF analysis is not readily clear and to be more certain of this improvement additional scatter or profilometry would be necessary.

Prior experience on more severe grazing aspheric optics has shown that the Flow-Polishing has produced surfaces that, when LSM coated for 14.5 angstroms, perform to the theoretical reflection and scatter level as tested in actual use.

Final Report Documentation:

Signature of Authorized Company Representative:



Phillip C. Baker

Position: President / Baker Consulting

Dated: 3/2/1992

SCREEN IMAGE USER=\*AGR SESSION=T20BR03 7/30/92-10:47:21-AM

DISPLAY 92N20515/2

92N20515\*# ISSUE 11 PAGE 1877 CATEGORY 70 RPT#: NASA-CR-184312 NAS  
1.26:184312 CNT#: NASA ORDER H-08082-D NASA ORDER H-11210-D 92/03/02  
25 PAGES UNCLASSIFIED DOCUMENT

UTTL: Advanced flow-polishing and surface metrology of the S056 X Ray Telescope  
TLSP: Final Report

CORP: Baker Consulting, Walnut Creek, CA.

SAP: Avail: NTIS HC/MF A03

CIO: UNITED STATES

MAJS: /\*GEOMETRICAL OPTICS/\*GRAZING INCIDENCE/\*METROLOGY/\*MIRRORS/\*SURFACE  
FINISHING/\*X RAY TELESCOPES

MINS: / ASPHERICITY/ CURVATURE/ LAYOUTS/ OPTIMIZATION/ SUBSTRATES/ WAVE FRONTS

ABA: Author

ABS: The surface finishing of X ray grazing incidence optics is a most  
demanding area of optical processing, both in terms of metrology and  
application of optical finishing techniques. An existing optical mirror  
was processed using a new removal technique that uses a jet of finely  
dispersed and extremely small particles that impact a surface, which under  
the correct conditions, produces an ultrasmooth surface, especially on  
aspheric curvatures. The surfaces of the S056 mirror are tapered conical  
shapes that have a continuously changing radius with the primary mirror  
having a parabolic shape and the secondary mirror a hyperbolic shape. An  
optical ray trace that was conducted of a telescope used the measured

ENTER:

MORE

SCREEN IMAGE    USER=\*AGR            SESSION=T20BR03            7/30/92-10:48:24-AM

DISPLAY 92N20515/2

parameters from the existing substrates to set up the prescription for the optical layout. The optimization indicated a wavefront performance of 0.10 A at 0.633 micron.

ENTER: